Sahlman, Mika; Aromaa, Jari; Lundström, Mari

Detachment and flow behaviour of anode slimes in high nickel copper electrorefining

Published in:
Physicochemical Problems of Mineral Processing

DOI:
10.37190/ppmp/186194

Published: 19/03/2024

Document Version
Publisher's PDF, also known as Version of record

Physicochem. Probl. Miner. Process., 60(2), 2024, 186194

http://www.journalssystem.com/ppmp

Physicochemical Problems of Mineral Processing

ISSN 1643-1049

Detachment and flow behaviour of anode slimes in high nickel copper electrorefining

Mika Sahlman, Jari Aromaa, Mari Lundström

Department on Chemical and Metallurgical Engineering, School of Chemical Engineering, Aalto University, Espoo 02150, Finland

Corresponding author: mari.lundstrom@aalto.fi (M. Lundström)

Abstract: Most of the world's copper is produced via copper electrorefining, where nickel is the most abundant impurity in the process. Previously it has been suggested that nickel affects the adhesion of anode slimes on the anode as well as the porosity of the slime layer that forms. This paper investigates the effects of nickel, oxygen, sulphuric acid and temperature on the detachment of anode slimes from the anode surface. The detachment of particles as a function of both anode and electrolyte composition was studied on laboratory scale using a camera connected to a Raspberry Pi, and particle detection and movement analysed using TrackPy. The results revealed four different slime detachment mechanisms: cloud formation, individual particle detachment, cluster detachment and avalanche. These were found to be dependent on the electrolyte (0, 10, 20, 30 g/dm^3 Ni^{2+} & 100, 200 g/dm^3 H_2SO_4), with increasing nickel concentration promoting cluster detachment and increasing sulphuric acid concentration favouring detachment of individual particles. Anode composition (0.05-0.44 wt% O and 0.07-0.64 wt% Ni) was shown to affect the flow direction of anode slimes, with increasing nickel leading to more upward-flowing slimes. Typical particle movement velocities were from -0.5 to 1.0 mm/s regardless of the electrolyte and anode composition, and regardless of the operating temperature (25 °C & 60 °C) for small particles (<0.5 mm). The results also support previous findings that increasing the nickel concentration of the electrolyte leads to a more porous anode slime layer on the anode.

Keywords: copper, electrorefining, anode slime, nickel, oxygen

1. Introduction

Over 80% of the world's high purity copper is produced by copper electrorefining (International Copper Study Group, 2022). However, as ore grades are becoming poorer and copper scrap is being used increasingly, refineries are faced with more impurities and challenges in production. Increased impurity levels also result in more anode slimes being generated. While anode slimes are a by-product of copper electrorefining that contains precious metals, these slimes are also known to have a negative effect on cathode quality. In addition, anode slimes may cause nodulation (Andersen et al., 1983; Dutrizac and Chen, 1999) leading to short-circuits, increased energy consumption, loss of production and further contamination. For these reasons, a lot of research has been done on the dependency between anode slimes and the nodulation phenomenon.

In copper electrorefining, a current is passed through an impure anode and pure copper is deposited on the cathode. As the copper anodes dissolve in the process, solid impurities within the anode emerge and form an anode slime on the surface of the anode. Previous studies on anode slime and its detachment have focused on its role in increasing the anode's potential, i.e. passivation, the growing slime layer inhibiting the diffusion of Cu^{2+} (Abe et al., 1980). Eventually, the oxygen evolution potential is reached and the anode slimes are dislodged by the oxygen evolution and either settle or remain in suspension (Ling et al., 1994a; Ling et al., 1994b; Gu et al., 1995). It has been suggested that the adherence of these slimes to the anode surface is affected by factors such as the anode composition, current density, temperature and electrolyte flow rate (Zeng et al., 2015a, 2015b; Zeng et al., 2016b, 2016a, 2017). The settling rate of the anode slimes is also affected by the electrolyte composition (Kalliomäki et al., 2019).

DOI: 10.37190/ppmp/186194

Past research has focused on the general detachment and slime flow behaviour in electrorefining but not on the effect of Ni on slime detachment and flow behaviour specifically.

Nickel is less noble than copper and thus the majority of the nickel dissolves into the electrolyte, although some of the Ni deports to the anode slimes as sulphates and oxides (Abe et al., 1980). While there is variance in electrorefining operations, average Ni^{2+} concentrations in the electrolyte have increased by over 50% in the last two decades, increasing from 9.7 g/dm^3 in 1999 to 15.3 g/dm^3 in 2022 (Moats et al., 2022). The exact cause behind the increase in nickel concentrations is complex. This is probably partly due to the decreasing ore grades in mining operations (Michaux, 2021), which are reflected in the downstream process, and partly due to the recycling of e-waste and nickel-rich copper scrap. In e-waste, Ni can be found for example in printed circuit boards (PCBs), which can contain up to 5.35 wt% Ni (Duan et al., 2011). Ni is also a common alloying element in copper products, used to produced corrosion-resistant cupronickels which typically have about 10% to 30% Ni. Integration of metal production value chains adds more complexity to the analysis as the impurity streams become mixed. In addition, Cu production capacities have increased over time (Moats et al., 2022) but the electrolyte bleed capacity, which is used to control the Ni^{2+} concentration of the electrolyte, may not have increased at the same rate.

It has been suggested that the presence of Ni^{2+} in the electrolyte leads to increased nodulation (Tetsuka and Okamoto, 2019) and increasing Ni^{2+} concentrations have been linked to decreasing current efficiency and dendrite growth in electrowinning (Ogawa, 2016). However, the exact mechanism by which nickel could influence contamination and nodulation is not fully understood. It is not clear how cationic impurities such as Ni^{2+} in the electrolyte could cause nodulation, and while anode slimes in general have been linked to nodulation, nickel-containing anode slimes have not caused nodulation, probably due to the resistive nature of nickel oxide (Andersen et al., 1983; Sahlman et al., 2021). This paper investigates the possible indirect ways that increased nickel concentrations may lead to nodulation, by influencing anode slime detachment and flow behaviour in electrorefining, as it has been suggested that Ni influences the structure of the slime layer that is formed (Jarjoura and Kipouros, 2006a). The focus in this paper is on the influence of specific impurities, i.e. nickel and oxygen, as well as the sulphuric acid concentration.

2. Materials and methods

The anode samples studied were cut from industrial anodes and polished with P400 emery paper. Anodes were analysed by a third party using ARL8860 iSpark OES (Thermo Fisher Scientific, United States) for metallic elements and TC-500 (Leco Corporation, United States) for oxygen. The chemical composition of the main elements in the anodes are presented in Table 1. All electrorefining experiments (Table 2) were performed with an electrolyte composition of 40 g/dm3 Cu^{2+} prepared by dissolving copper sulphate pentahydrate (technical grade, VWR Chemicals, Belgium) in ion-exchanged water. The desired H_2SO_4 concentration was achieved by adding 95% sulphuric acid (technical grade, VWR Chemicals, Belgium). The nickel concentration in the electrolyte was varied (0-30 g/dm3) and was added as nickel sulphate hexahydrate (98%, Alfa Aesar, Germany) and the temperature was varied between 25 °C and 60 °C. Experimental parameters reflect common electrorefining conditions with the current density being on the high-end (Moats et al. 2022). H_2SO_4 concentration was lowered to 100 g/L in some of the experiments to determine if the acid concentration may affect the anode slime structure. Some of the experiments were performed at 25°C because major slime detachment could not be observed in the absence of passivation, and the temperature was lowered to accelerate the anode passivation.

Laboratory-scale copper electrorefining experiments (Table 2) were performed in a cylindrical 200 ml jacketed cell. Stainless steel (EN 1.4301, X5CrNi18-10) was used as the working electrode and industrial Cu anode pieces (Table 1) were used as the counter electrodes. A single junction Ag/AgCl (+199 mV vs SHE, Pine Research, United States) was used as the reference electrode. 1M KCl gel was used to protect the reference electrode and a salt bridge was used to protect the gel from the cell temperature. The gel was prepared by dissolving KCl (analytical reagent, Riedel-de Haën, Germany) in ion-exchanged water with agar (bacteriological grade, Amresco, United States), heating the solution and allowing it to cool down in extension tubes. The backs and sides of the electrodes were covered with

non-conductive tape. The anodes and cathodes were approximately 2.3 cm wide and 3.9 cm tall. A thin region (3 mm for one-day experiments, 5 mm for five-day experiments) was left visible on the anode sides to monitor anode slime detachment. A constant current density of 350 A/m² was supplied by a

Table 1. Anode compositions for six studied anodes (AN-1-6)

Element	AN-1	AN-2	AN-3	AN-4	AN-5	AN-6
Cu (wt%)	99.5	99.2	98.8	98.5	98.2	98.5
As (wt%)	0.01	0.11	<0.003	<0.003	0.58	0.29
Ni (wt%)	0.047	0.073	0.29	0.33	0.64	0.61
O (wt%)	0.12	0.28	0.099	0.29	0.35	0.44
Pb (wt%)	0.085	0.13	0.13	0.11	0.070	0.040
Sb (wt%)	0.018	0.047	0.11	0.050	0.075	0.031
Sn (wt%)	<0.003	0.006	0.018	0.008	0.007	0.010
Te (wt%)	<0.003	<0.003	0.040	0.029	0.010	<0.010

Table 2. Experimental series, where EE indicates varying electrolyte compositions and AE varying anode compositions. All experiments used 40 g/dm³ of Cu^{2+} (except EE-5). Current density was a constant 350 A/m² in all the experiments. *The initial results of the CEE series were presented at Copper2022 (Sahlman et al., 2022)

Experiment	Anode	c(Ni, anode, wt%)	c(O, anode, wt%)	c(Ni^{2+}, electrolyte, g/dm³)	c(H_2SO_4, electrolyte, g/dm³)	Temperature (°C)
CEE-1*	AN-5	0.64	0.35	0	100	25
CEE-2*	AN-5	0.64	0.35	10	100	25
CEE-3*	AN-5	0.64	0.35	20	100	25
CEE-4*	AN-5	0.64	0.35	30	100	25
EE-1	AN-5	0.64	0.35	0	200	25
EE-2	AN-5	0.64	0.35	10	200	25
EE-3	AN-5	0.64	0.35	20	200	25
EE-4	AN-5	0.64	0.35	30	200	25
EE-5	AN-5	0.64	0.35	0 (60 g/dm³ Cu^{2+})	100	25
AE-1	AN-1	0.12	0.047	0	200	25
AE-2	AN-2	0.073	0.28	0	200	25
AE-3	AN-3	0.29	0.099	0	200	25
AE-4	AN-4	0.33	0.29	0	200	25
AE-5	AN-6	0.61	0.44	0	200	25
EE-1.2	AN-5	0.64	0.35	0	200	60
EE-2.2	AN-5	0.64	0.35	10	200	60
EE-3.2	AN-5	0.64	0.35	20	200	60
EE-4.2	AN-5	0.64	0.35	30	200	60
AE-1.2	AN-1	0.12	0.047	0	200	60
AE-4.2	AN-4	0.33	0.29	0	200	60

potentiostat (Iviumstat.XRe, Ivium Technologies, Netherlands). A data logger (Grant Squirrel 2020, Grant Instruments., United Kingdom) was connected to the electrodes to collect the anode, cathode and cell potential data. A dual colour LED panel (LEDP120C, Godox, China) was placed behind the electrorefining cell. The panel was perpendicular to the anode and cathode to illuminate the detaching anode slime particles. A Raspberry Pi HQ camera connected to a Raspberry Pi (Raspberry Pi Foundation, United States) was used to record the experiments. Two 5 mm extensions rings and four close-up lenses (1+2+2+4 diopter) were connected to the 16 mm telelens of the camera. Video recording was performed at 10 frames per second with a shutter speed of 0.1 seconds and a resolution of 1600x1200 pixels using open-source software (Miikki and Karakoc, 2020). A schematic of the experimental setup is shown in Fig. 1.

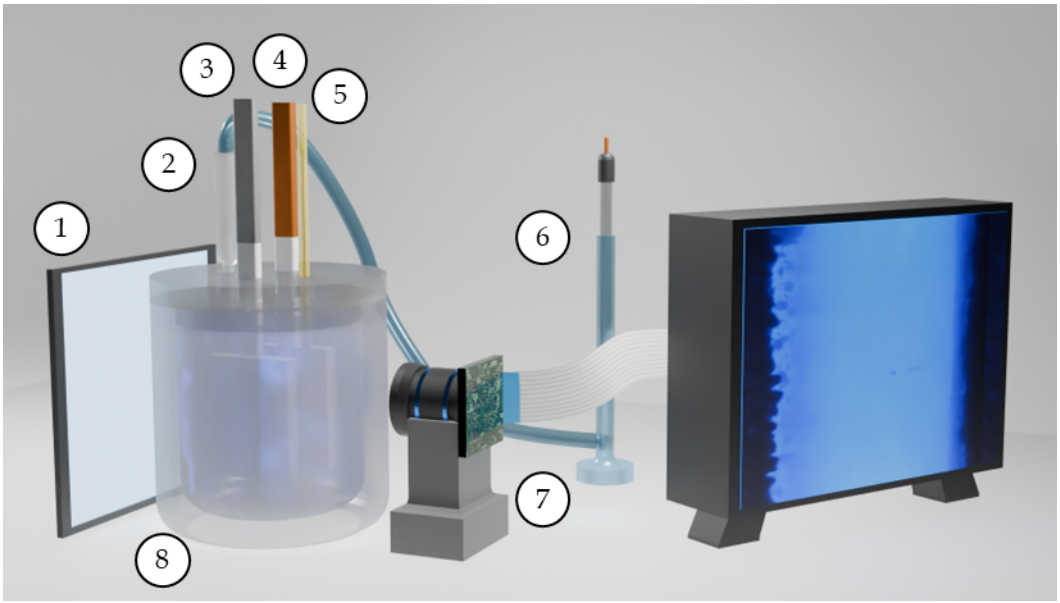

Fig. 1. A simplified schematic of the experimental setup. 1) a dual colour LED panel, 2) A salt bridge. 3) cathode, 4) anode, 5) thermometer, 6) a single junction Ag/AgCl the reference electrode surrounded by a KCl-agar gel, 7) A Raspberry Pi HQ camera connected to a Raspberry Pi with screen, 8) A jacketed reactor

Particle tracking was done after the experiments and the trajectories of the settling anode slime were detected and analysed using the TrackPy Python package (Allan et al., 2021). The detection of particles and the calculation of trajectories was computed with Triton, a high-performance computing cluster. The detection parameters were set to 21, 1000, 'True' and 'numba' for diameter, minmass, invert and engine, respectively. The diameter parameter is the expected size of the features. Minmass is the minimum integrated brightness and is used to eliminate spurious features. The algorithm detects bright features and invert is used to invert the original dark features (anode slime). The engine parameter sets the Python compiler. (Allan et al., 2021) Detected particles were linked to trajectories and, in cases where a particle disappeared temporarily due to light fluctuations or loss of focus, the particles were kept in the memory for 30 frames and relinked to the trajectory. Trajectories that lasted less than 2 seconds were excluded from the analysis. To remove artefacts caused by light fluctuations and glass imperfections as well as false detections within large black areas, the data was further filtered for trajectories moving slower than 0.05 mm/s or that had a total displacement of less than 4 mm. Particle velocities were calculated based on the first and last known location of the particle.

3. Results and discussion

3.1. General observations on anode slime detachment mechanisms and flow behaviour

Typically, settled anode slimes have particle sizes of 1-120 µm (Kalliomäki et al., 2019), and thus any observed slime with a larger particle size is likely to be a cluster of several individual particles. However, in this paper particles which are 0.1-0.5 mm in diameter are considered as individual

particles, whereas anything larger is considered a cluster. Clusters were observed to be 0.5-7 mm in diameter. 'Individual particles' as classified in this paper had a roughly spherical shape and no gas bubbles were seen within them. Clusters were sometimes observed to have entrapped significant amounts of gas bubbles (Fig. 1S).

Four different detachment mechanisms (Table 3) had been previously identified from recorded videos (Sahlman et al., 2022), and were verified in the current study. The mechanisms were observed to be influenced by both the electrolyte and anode composition as well as temperature. In *Cloud formation* (Fig. 2A), the anode passivates, and the forming bubbles push out microscopic anode slime particles, resulting in the formation of an anode slime cloud. *Cloud formation* was especially associated with high impurity anodes (AN-5 & AN-6). At 25 °C, large-scale *Individual particle detachment* (Fig. 2B) was more commonly observed with low impurity anodes (AN-1, AN-2, AN-3 & AN-4) and/or 200 g/dm^3 sulphuric acid concentration, while with 100 g/dm^3 H_2SO_4, *individual particle detachment* was seen typically after other forms of detachment had occurred. At 60 °C, solitary individual particles were observed to detach independently from the anode sometimes. *Cluster detachments* (Fig. 2C) were more commonly observed with high impurity anodes than with low impurity anodes. At 25 °C, intact slime layers were pushed off by the oxygen evolution, with bubbles entrapped within the slime, whereas at 60 °C clusters simply detached without any effect on the anode potential. At 25 °C, *Cloud formation*, *Individual particle detachment* and *Cluster detachment* were all associated with passivation, while *Avalanches* (Fig. 2D) were less common and occurred only when the slime layer grew thick enough.

Table 3. Observed detachment mechanisms and their descriptions

Detachment mechanism	Description
Cloud formation (Fig. 2A)	Cloud of microscopic particles and bubbles in the vicinity of anode surface.
Individual particle detachment (Fig. 2B)	Spherical particles with a diameter of 0.1-0.5 mm.
Cluster detachment (Fig. 2C)	A large mass of connected particles forming various shapes with diameters of about 0.5-7 mm.
Avalanche (Fig. 2D)	A collapsing slime layer that falls directly down the anode surface.

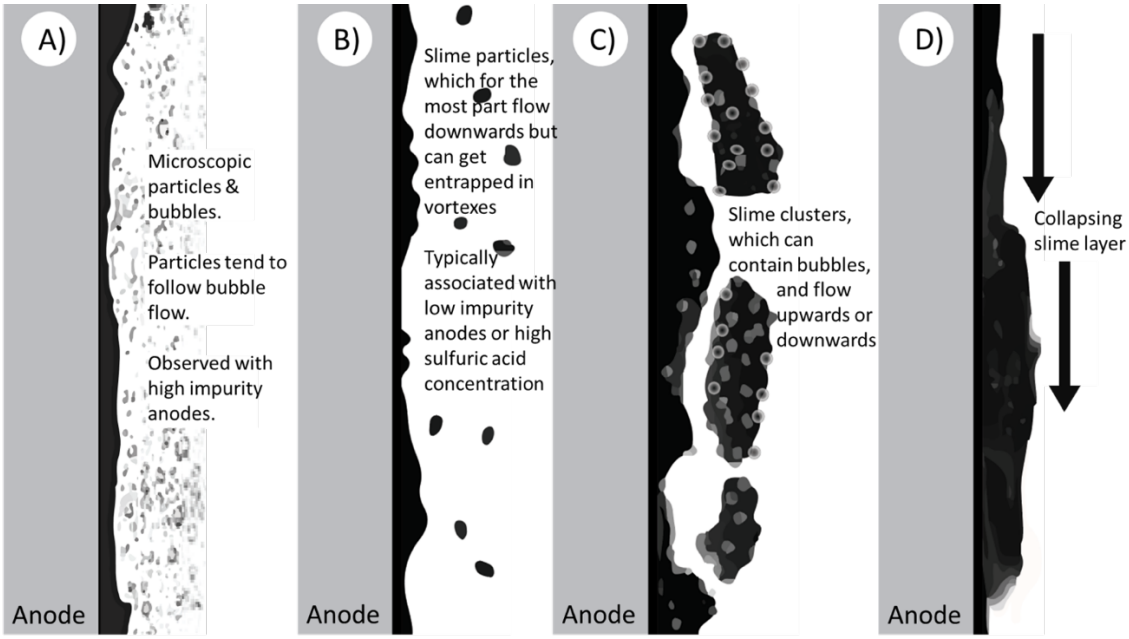

Fig. 2. Schematic of anode slime detachment mechanisms: (A) Cloud formation. (B) Individual particle detachment from the anode surface. (C) Cluster detachment. (D) Avalanche – Slime surface detaches like an avalanche from the surface

Passivation occurred in all the experiments performed at 25 °C, but it was not observed at the higher temperature investigated (60 °C). When the high impurity anodes (AN-5 & AN-6) passivated, slime detachment started with *Cloud formation*. Microscopic particles (diameter <0.1 mm) formed clouds in the vicinity of the anode surface that could either rise up along the bubbles or slowly settle. *Individual particle detachment* could be observed after passivation with low impurity anodes (AN-1, AN-2, AN-3 & AN-4) and along with *Cluster detachment*. Instances of *Cluster detachment* were observed with thicker slime layers and bubbles could occasionally be seen stuck in the slime clusters. At 25 °C, *Cluster detachment* was also always associated with a drop in anode potential. *Avalanche* is a type of cluster detachment which did not always result in a drop in anode potential and avalanches did not remove the entire slime layer. This indicates that *avalanche* detachment is more related to the mass and structural integrity of the slime layer rather than passivation and oxygen evolution.

Ling, Z. H. Gu and Fahidy (1994) have reported that slime particles exhibited random movement trajectories as they settled. The electrolyte flow between the electrodes has been suggested to be able to carry anode slime towards the cathode (Zeng, Werner and Free, 2015), and, depending on the particle size, the electrolyte flow may significantly influence the settling rate and direction of slimes (Ling, Z. H. Gu and Fahidy, 1994; Zeng, Wang and Free, 2016a). In the current study, some of the slimes showed random movement at times (Fig. 3A) but for the most part the slime movement trajectories were predictable, with particles flowing straight in one direction (Fig. 3B). While particles could be moved by the electrolyte flow, natural convection was not observed to be able to carry slime particles to the cathode (Fig. 3A) and the slime particles were seen moving upwards (Fig. 3B) near the centre of the gap between the anode and the cathode. In addition, it was observed that particle movement could be random with larger slime clusters and at the same time tiny individual particles could settle straight downwards (Fig. 4), which indicates that the anode slime cluster composition might influence the settling behaviour more than the electrolyte flow.

While it has been reported that detaching slime would eventually occupy 80% of the electrolyte volume (Gu, Chen and Fahidy, 1995), in the current study most of the slime resided near the anode surface, the particles did eventually settle and the electrolyte remained relatively clear. The horizontal velocity profiles aggregated from all of the experiments (Fig. 5) follow a normal distribution, which further supports the conclusion that natural convection does not have a major impact on the movement of the majority of slimes. This is supported by the fact that the camera was placed to video-record the bottom half of the anode side of the cell, and if natural convection affected the slime movement the distribution should skew more towards the negative velocities. The vertical velocity data in Fig. 6 is more representative of high impurity electrolysis, because there was more slime generation with high impurity anodes and electrolyte, but for horizontal velocity the profile is appropriate for both low and high impurity electrorefining (see Figs. 2-3S).

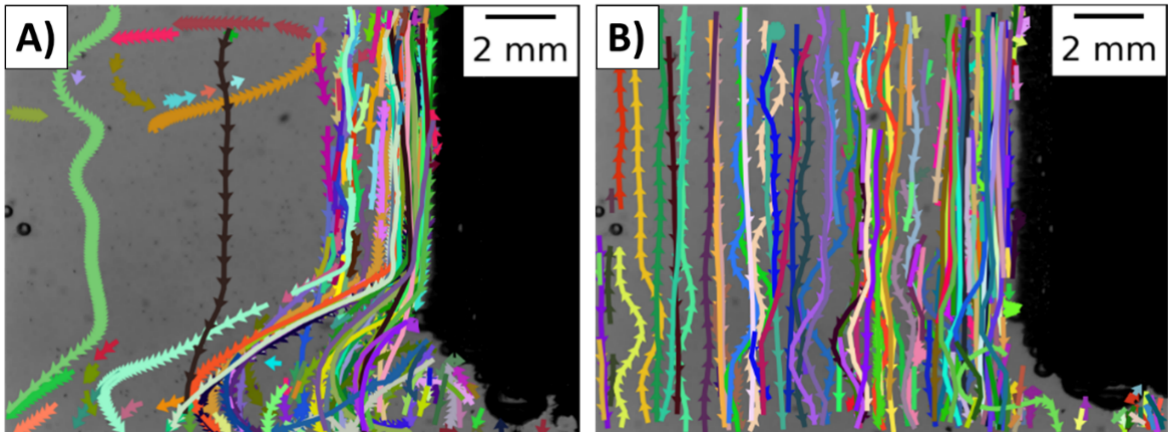

Fig. 3. Observed settling behaviour of anode slimes from AE-3.1. A) Trajectories from t = 10.5 h to t = 11 h. B) Trajectories from t = 6.5 h to t = 10.2 h. The distance between the anode (black body on the right) and the cathode is approximately 2 cm. The left side of the images is approximately 1 cm from the anode. A higher frequency of arrows indicates slower movement. Visible particles that do not overlap any trajectories are slime particles and bubbles which have adhered to the reactor glass. These detections have been filtered from the results

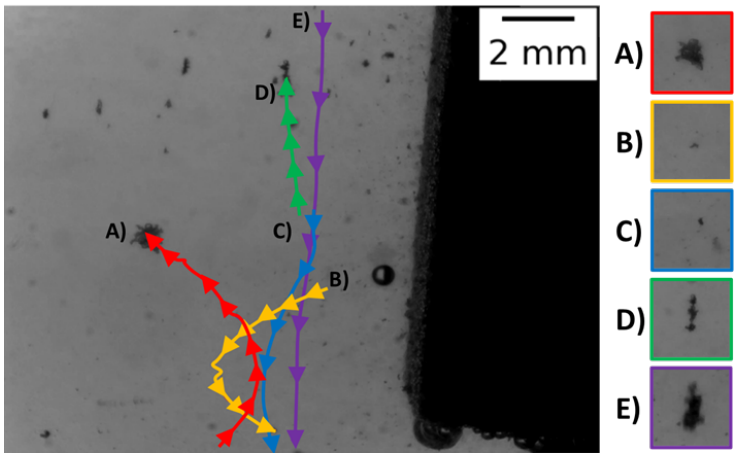

Fig. 4. Effect of particle size on slime movement trajectories and settling rates. The selected trajectories are taken from AE-4 after 9.44 hours of electrolysis and represent movement that occurred over 50 seconds. A) Roughly spherical cluster which had a vertical velocity of -0.12 mm/s. B) Individual particle which had a vertical velocity of 0.08 mm/s. C) Individual particle which had a vertical velocity of 0.33 mm/s. D) Stick-like cluster which had a vertical velocity of -0.08 mm/s. E) Cluster which had a vertical velocity of 1.41 mm/s. Negative velocities indicate movement is upwards and positive velocities mean that the particle is settling downwards

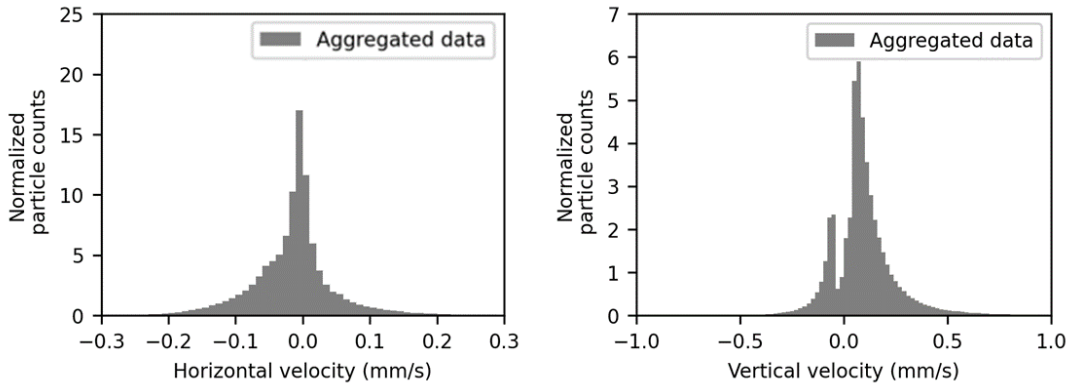

Fig. 5. Horizontal (left) and vertical (right) velocity profiles aggregated from the velocities across all experiments. Detection of particles at the bottom corner of the anode. Negative horizontal velocities indicate movement towards the cathode and positive horizontal velocities indicate movement towards the anode. Negative vertical values mean the particle is flowing upwards and positive vertical velocity means the particle is settling downwards. Velocities were calculated based on the first and last point of detection for each trajectory

3.2. Effect of electrolyte composition on slime settling

At a sulphuric acid concentration of 100 g/dm^3, slime detachment is clearly linked to passivation, as particle detection is associated with drops in the anode potential (Fig. 6). The magnitude of the potential drop varied between experiments, and larger drops seemed to result from bigger slime amounts detaching from the surface. Increasing the nickel concentration from 0 g/dm^3 to 10 g/dm^3 was shown to increase the frequency of small drops in potential and further increases in nickel concentration (to 20 g/dm^3 and 30 g/dm^3) increased the magnitude of the drops in potential (Fig. 6). This is probably related to the types of slime masses formed and detaching from the surface, with larger masses causing bigger drops in potential. Increasing the sulphuric acid concentration to 200 g/dm^3 altered the slime detachment mechanism. Slime detection could no longer be clearly linked to anode passivation and partial depassivation. Clusters up to a diameter of about 2 mm were still observed but the majority of the detections can be considered to be individual particles, resulting in a large number of particle counts (Fig. 6). Increasing the sulphuric acid concentration is predicted to degrade the anode slime layer, causing the slime to detach as individual particles and small clusters.

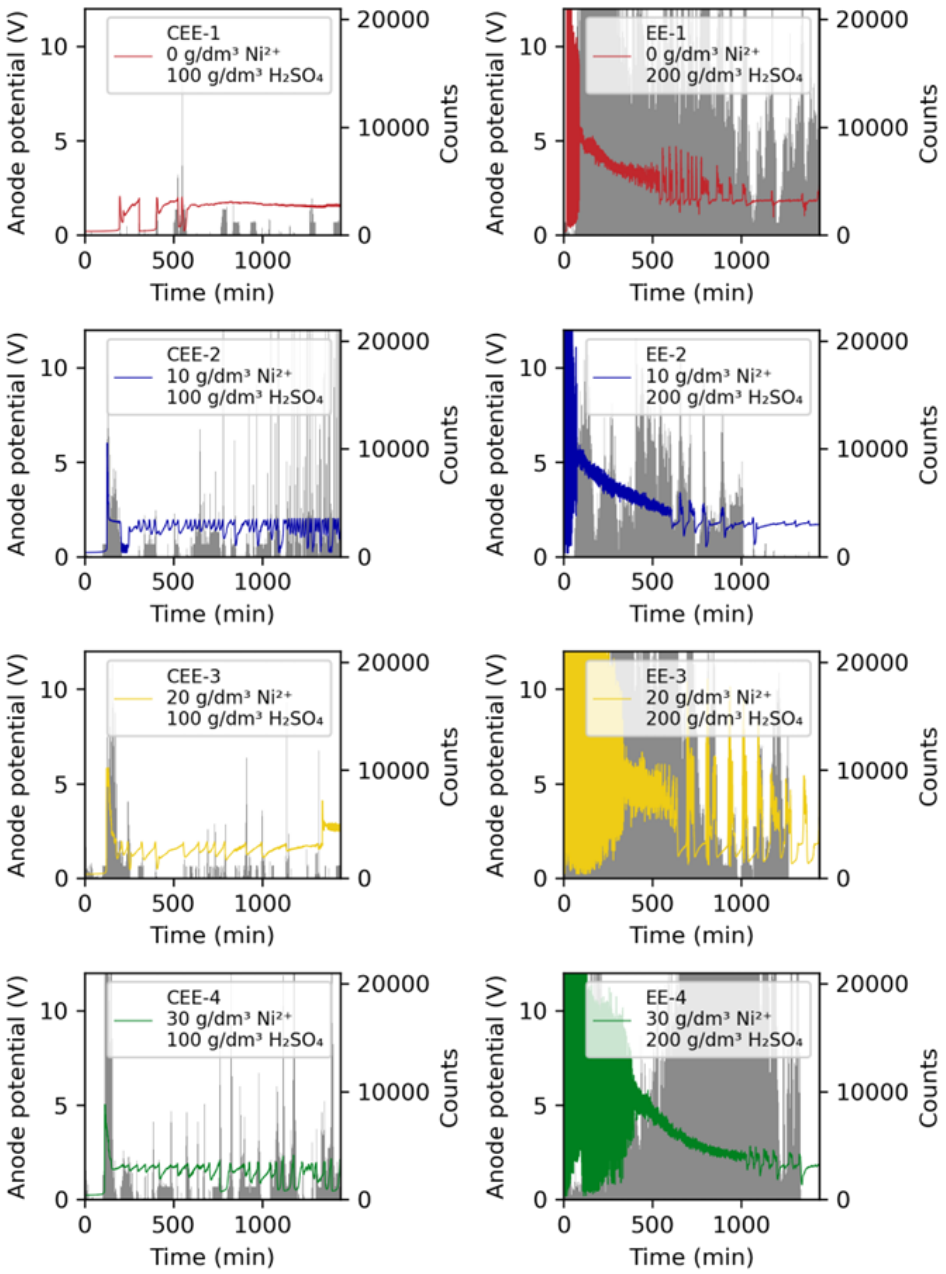

Fig. 6. Anode potential (vs Ag/AgCl) and number of detected slime particles as a function of time. Electrolyte composition: 100 g/dm³ sulphuric acid (left) and 200 g/dm³ (right), Ni^{2+} = 0, 10, 20 & 30 g/dm³ from top to bottom. *Initial results of CEE series were presented in Sahlman et al. (2022). Previous unfiltered particle trajectories were treated based on exceeding both particle displacement *and* velocity thresholds; in contrast, the current results are filtered based on exceeding either the displacement *or* the velocity threshold. Thus, slowly moving solid suspensions are better represented in the current results

The effect of Ni^{2+} is not as evident at the higher (200 g/dm³) sulphuric acid concentration as it is with the lower (100 g/dm³) concentration. This can be seen in Fig. 7, which shows examples of anode slime detachment around the midpoint of the experiments (10-14 h of electrolysis). At the lower sulphuric acid concentration bigger clusters can be observed as the Ni^{2+} concentration increases, but at the higher acid concentration the anode slimes form smaller clusters and individual particles. While Ni^{2+} still probably causes the anode slime layer to be more porous, the influence of sulphuric acid causes the porous structures to degrade. In fact, it is possible that the increased porosity of the slime layer makes it easier for sulphuric acid to dissolve the integral structures of the slime layer. This might result in structures that cannot hold gas bubbles or are too dense to float upwards.

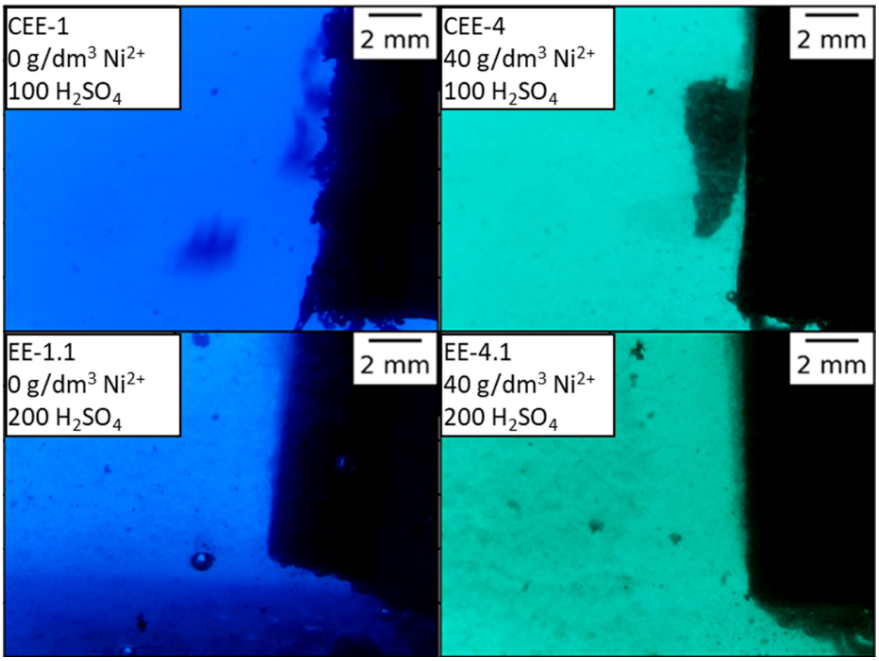

Fig. 7. Typically observed anode slime detaching from the anode surface in the middle stages of electrorefining (10-15 h) at room temperature during 24 hours of electrolysis

Despite influencing the predominant particle detachment mechanism, the electrolyte composition had no impact on the horizontal flow behaviour of the anode slime particles, even though it could be expected that individual particles would be more likely to follow the natural convection of the electrolyte. Instead, the horizontal velocities followed a normal distribution, similar to that shown in Fig. 6, with most horizontal velocities being in the range of -0.2 - 0.2 mm/s (Fig. 2S). However, the electrolyte composition did affect the settling rate, i.e. vertical velocities of the anode slime particles.

At 100 g/dm^3 sulphuric acid concentration, increasing the nickel concentration led to more upward-flowing particles (Fig. 8). Ni^{2+} has been suggested to increase the porosity of the slime layer (Jarjoura and Kipouros, 2006a) and at 100 g/dm^3 sulphuric acid concentration the increasing upward flow might partially explain this observation. Increasing porosity enables bubbles to be entrapped in the slime, which could partly explain the increased upward flow. Increasing porosity also decreases the density of the detaching slime, and combined with the increasing electrolyte density, a more upward flow of particles could be expected. The velocity profiles shown in Fig. 8 contain all the detected particle trajectories. When the vertical velocity data is filtered of slime detections that occurred near the surface (~1 mm from anode surface), nearly all the upward-flowing particles disappear with 100 g/dm^3 sulphuric acid concentration in the electrolyte (Fig. 9). This further indicates that the upward flow is indeed caused by the bubbles from oxygen evolution attaching to the porous anode slime layer, or individual particles attaching to the bubbles, as in flotation. Interestingly, with a sulphuric acid concentration of 200 g/dm^3 there is no major change in the particle flow behaviour of particles when the surface trajectories are ignored (Fig. 9). It is likely that sulphuric acid degrades the slime layer on the anode surface and prevents the formation of large stable clusters which can entrap gas, and instead smaller slime clusters and individual particles detach. Increasing the sulphuric acid concentration also increases the density of the electrolyte, which, when combined with smaller particle and cluster sizes, might lead to a higher proportion of particles flowing upwards. This might result in the upward slime flow that is observed throughout the electrolyte and not only on the surface.

The detected detachment of anode slime occurred during anode passivation, and increasing Ni^{i2+} has been associated with passivation. While Ni^{2+} may decrease the time for passivation to occur, it has been suggested that passivation is more a result of the SO_4^{2-} anion than the Ni^{2+} cation (Moats, 1998). The effect of SO_4^{2-} and change of cation is shown in Fig. 10; interestingly, with similar total sulphate concentrations the slime flow behaviour is more similar to EE-1 than to CEE-3 when the cation is Cu^{2+} instead of Ni^{2+}. The fraction of upward moving particles near the anode surface is significantly less in

the absence of Ni^{2+}. The type of typical particles detaching from the surface also differs when the cation is changed. In similar sulphate concentrations, in the absence of Ni^{2+} particles detach typically as individual particles, as they do in 200 g/dm³ H_2SO_4, whereas large clusters can be observed in the presence of Ni^{2+} and with a lower total SO_4^{2-} concentration (Fig. 11). These observations suggest that Ni^{2+} does have an effect on slime detachment.

Ni^{2+} slightly increases the density and viscosity of the electrolyte (Kalliomäki et al., 2017, 2019) but the effect on settling rates is predicted to be linear (Fig. 12) and high nickel concentrations should lead to slower settling rates. However, the observations in the current study contradict these predictions, as the typical slime settling rates were found to be 0-1.5 mm/s (Table 1-3S) regardless of the electrolyte composition. The results show that the maximum and average velocities are unaffected by the nickel and sulphuric acid concentrations, while upward moving velocities (i.e. 'minimum' velocities) increase slightly with increasing nickel and sulphuric acid concentration. Furthermore, the observed particle and cluster sizes were >0.1 mm (up to several mm) and their settling rates were of the same order of magnitude as the <0.1 mm particles on which the models are based.

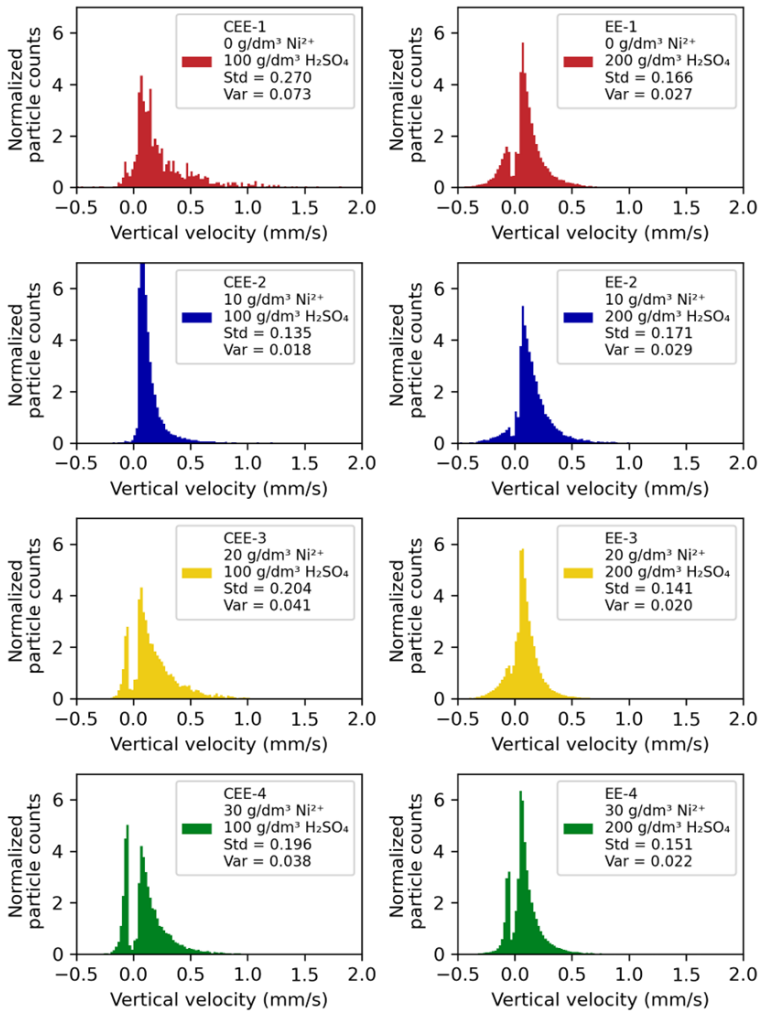

Fig. 8. Vertical particle velocities with increasing Ni and sulphuric acid concentration of the electrolyte. Negative values indicate upward movement towards the electrolyte surface. Particle counts have been normalized. Electrolyte composition: 100 g/dm³ sulphuric acid concentration (left) and 200 g/dm³ sulphuric acid concentration (right), Ni^{2+} = 0, 10, 20 & 30 g/dm³ from top to bottom. Negative values indicate movement upwards and positive values indicate settling downwards. Histogram bin sizes are 0.01 mm/s. *The initial results of the CEE series were presented in Sahlman et al. (2022). Previous unfiltered particle trajectories were treated based on exceeding both particle displacement and velocity thresholds; in contrast, the current results are filtered based on exceeding either the displacement or the velocity threshold. Thus, slowly moving solid suspensions are better represented in the current results

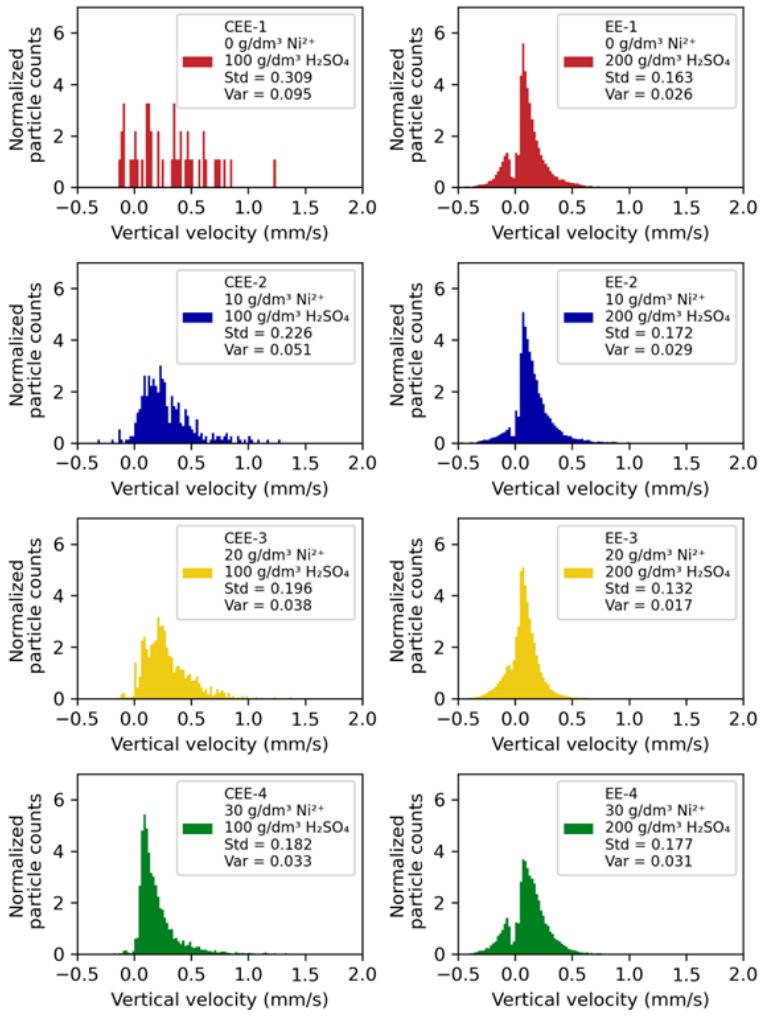

Fig. 9. Vertical particle velocities when detections within 1 mm of the anode surface are ignored. Negative value indicates upward movement towards the electrolyte surface Electrolyte composition: 100 g/dm³ sulphuric acid concentration (left) and 200 g/dm³ sulphuric acid concentration (right), Ni^{2+} = 0, 10, 20 & 30 g/dm³ from top to bottom. Negative values indicate movement upwards and positive values indicate settling downwards. Histogram bin sizes are 0.02 mm/s

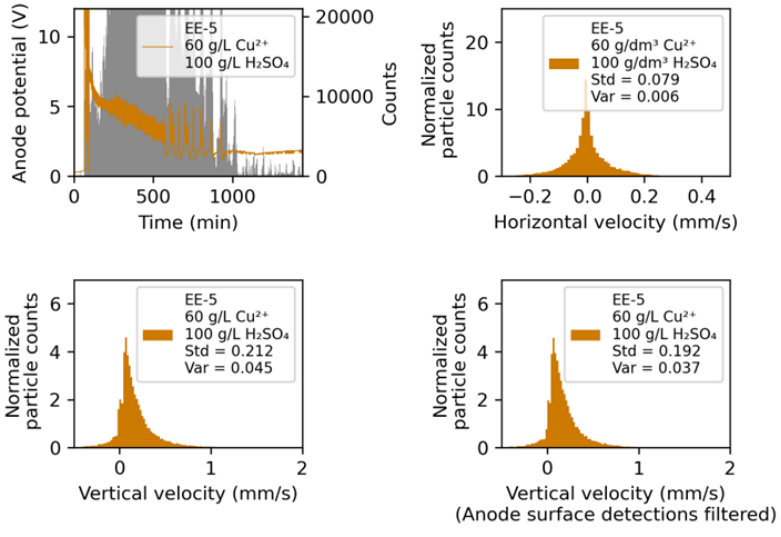

Fig. 10. Anode slime detachment and flow behaviour in the absence of Ni^{2+} and with elevated Cu^{2+} concentration. Total sulphate concentration: $SO_4^{2-} \approx 2$ mol/dm³, which is comparable to the CEE-3 sulphate concentration

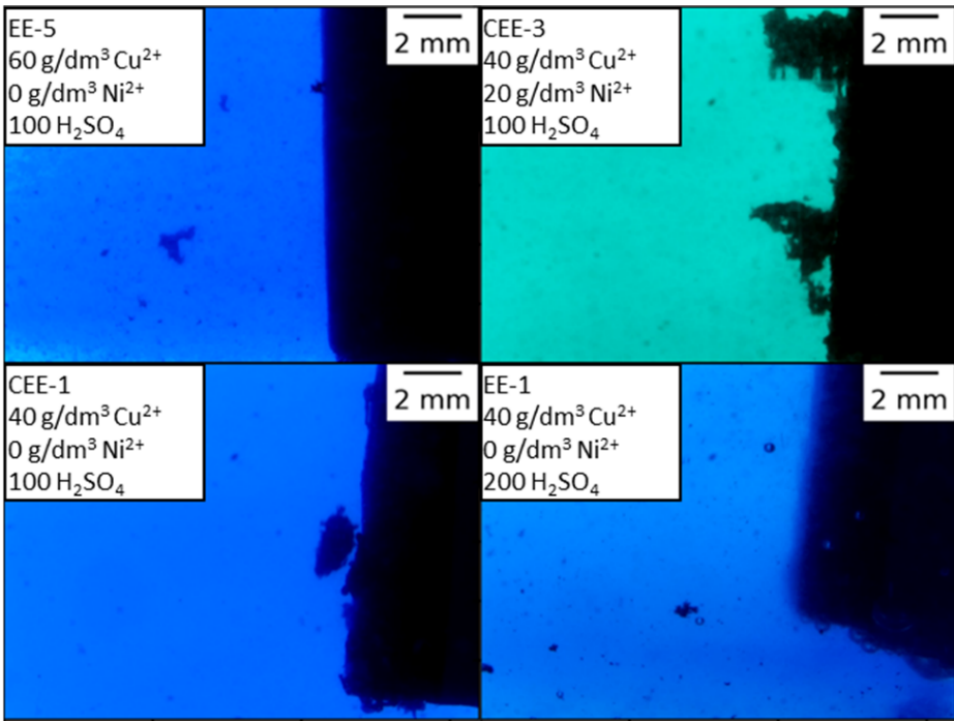

Fig. 11. Anode slime detachment and slime types in different SO_4^{2-} concentrations (about 2 mol/dm³ for EE-5 and CEE-3, respectively, and about 1.7 mol/dm³ and 2.7 mol/dm³ for CEE-1 and EE-1, respectively)

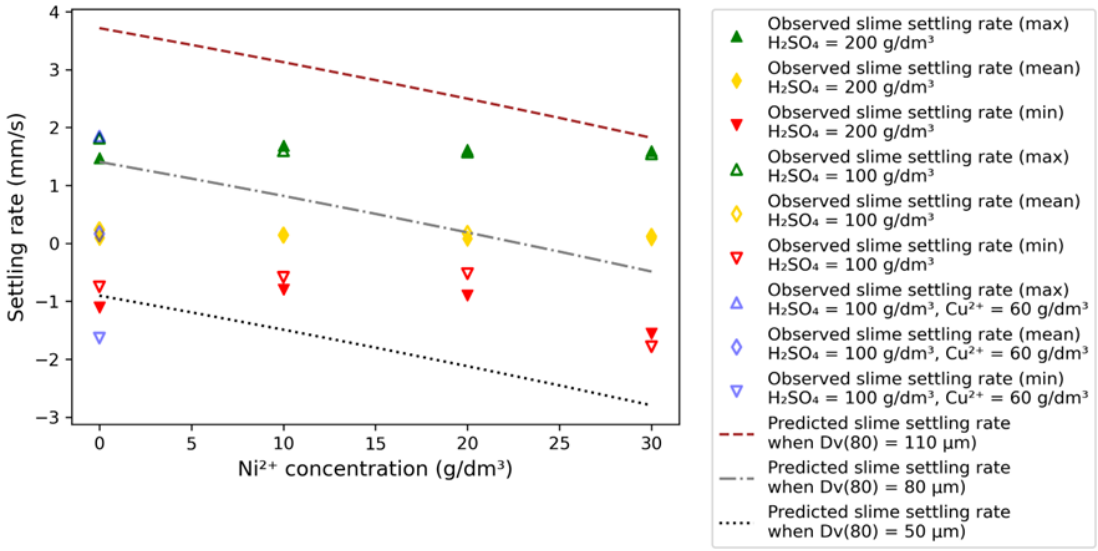

Fig. 12. Comparison of the observed room temperature settling rates as a function of nickel versus prediction models. The settling rate, density and viscosity predictions are based on the high sulphuric acid concentration models by Kalliomäki et al. (2019). The models are based on an electrolyte with 40 g/dm³ Cu^{2+}, 200 g/dm³ H_2SO_4 and a temperature of 25 °C. Exact values for the observed settling rate results are provided in Table 3S

Anode slime velocities are affected by the viscosity, but the direction of the movement should be affected by the densities of both the electrolyte and slimes. Given that some of the particles flow upwards, their density is lower than the density of the electrolyte. Although the density of real anode slime varies, with $CuSO_4$, $NiSO_4$, Cu_2O and NiO as some of the major components in anode slimes (Chen and Dutrizac, 1990), the slime densities are expected to be in the range of 3.6 - 6.7 g/cm³. This further indicates that the anode slimes are in fact more porous and thus less dense due to the electrolyte as the electrolyte density is in the range of 1.2 - 1.3 g/cm³ (based on the density model by Kalliomäki et al., 2019).

3.3. Effect of anode nickel and oxygen on slime settling

With low impurity anodes (AN-1, AN-2, AN-3 & AN-4), anode slime was observed to detach mainly as individual particles and small clusters, but with high impurity anodes (AN-5 & AN-6) *cloud formation* was also observed to occur at the anode surface (Fig. 13). The increased number of clusters and individual particles could be due to the type of impurities in the anode or simply a matter of more slime being generated and a side effect of a bigger slime layer. In-depth analysis on the main cause is complicated because the amount and type of anode impurities affect the slime generation. For example, as the Ni and O concentration increase in the anode, instead of dissolving into the electrolyte, Ni starts to form oxides which generate slime (Abe et al., 1980; Forsén, 1985; Chen and Dutrizac, 1990).

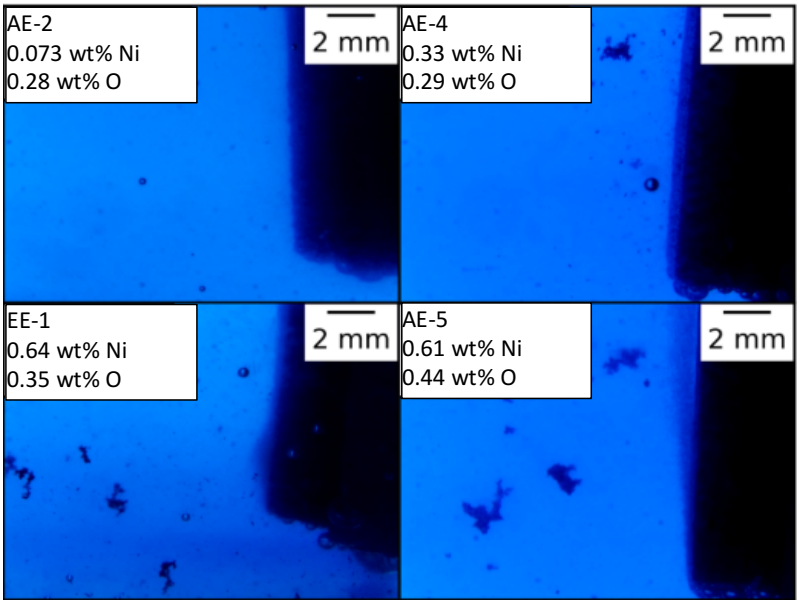

Fig. 13. Effect of increasing impurity levels on detaching slime masses. *Cloud formation* can be observed at the anode surfaces of EE-1 and AE-5, which used the anodes with the highest impurity concentrations

As with electrolyte composition, anode composition was shown not to influence the horizontal velocities, and most horizontal velocities are in the range of -0.2 - 0.2 mm/s (Fig. 3S). As with the electrolyte, the anode composition does not significantly affect the minimum, maximum and average settling rates (Fig. 14), but it does influence the vertical velocity profiles of anode slimes. Anode nickel has a major detrimental effect on the settling of anode slimes, as significantly more upward flow is observed when the nickel concentration increases from ~0.1% to ~0.3% (Fig. 15). This effect occurs with both oxygen levels ~0.1% and ~0.3%, with the velocity profiles being identical in both cases. It is impossible to determine whether the upward moving particles contain nickel, and the exact reason why increasing the anode nickel concentration leads to more upward movement is unclear.

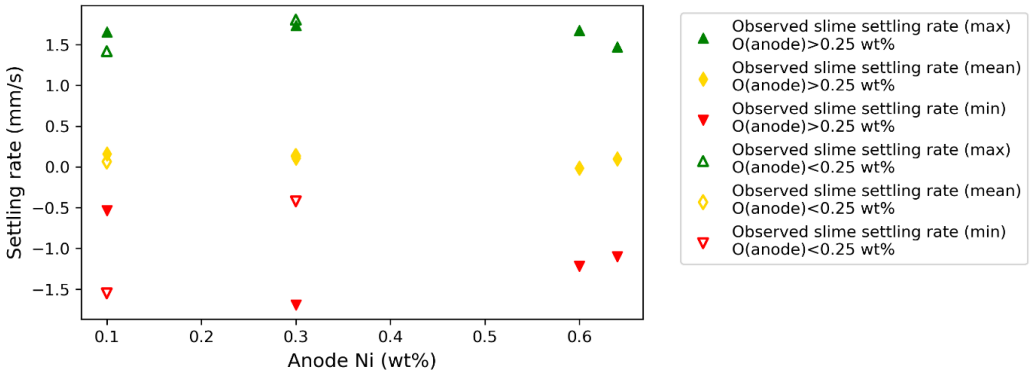

Fig. 14. Comparison of the observed room temperature settling rates as a function of anode nickel concentration versus the prediction models. Exact values for the observed settling rate results are provided in Table 3S

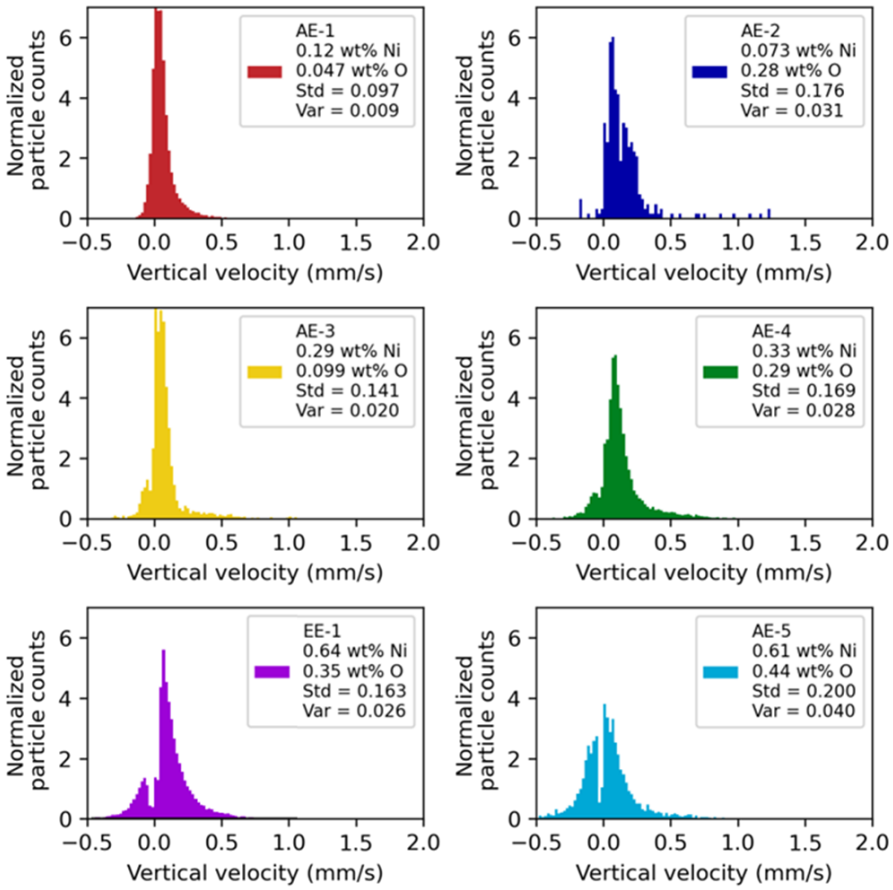

Fig. 15. Vertical particle velocities with increasing Ni and O in the anode without detection within 1 mm of the anode surface. A negative value indicates upward movement towards the electrolyte surface. Histogram bin sizes are 0.02 mm/s

Nickel in the anodes is known to form nickel oxide when the nickel concentration is ~0.3 wt% (Forsén, 1985), and the phenomenon could be related to the formation of nickel oxides, since it does not occur at lower nickel levels. However, it has been suggested that anode nickel decreases the porosity of the anode slime layer because of the low porosity factor of NiO (Jarjoura and Kipouros, 2006b). Decreasing porosity and a denser slime layer could be expected to improve slime settling, which contradicts the observed results. That being said, it should be noted that, even though the preconditions for NiO formation have been reached, most of the Ni remains in metallic form (Chen and Dutrizac, 1990) and the deportment of nickel to the anode slimes is dependent on the oxygen level of the anode (Abe et al., 1980). Based on the results of Abe et al. (1980), the deportment of nickel to the anode slimes (i.e. conversion of metallic Ni into oxides and precipitated sulphates) in this study should be <1%, ~10% and ~40% for anode oxygen levels of ~0.1 wt%, ~0.3 wt% and ~0.4 wt%, respectively, with high oxygen levels favouring NiO formation over kupferglimmer (Chen and Dutrizac, 1990). The presence of kupferglimmer is possible in some of the experiments (EE-1, AE-3, AE-4, and AE-5) as the Ni and Sb concentrations in the anode are above the thresholds of >0.25 wt% and >0.02 wt%, respectively (Chen and Dutrizac, 1990). However, the results cannot be attributed to kupferglimmer, given that the portion of upward moving slime is similar for both AE-3 and AE-4 in Fig. 16, and kupferglimmer is expected to be the favoured form in AE-3 and NiO in AE-4.

According to Hanus (1987), Ni improves the adhesion of anode slimes on anodes, and it could be that Ni also improves the internal adhesion of slime particles as well, which would make the porous structures more stable, and this would in turn cause the slime to flow upwards. This would explain the increased upward flow at lower oxygen concentrations where over 90% of the nickel is expected to be in metallic form. There is a major increase in the portion of upward moving particles when Ni and O concentrations are 0.6 wt% and 0.44 wt%, respectively (Fig. 16). At this point ~40% of the Ni is expected

to be in the slimes, mostly as NiO, but from the results it is impossible to determine whether NiO is the root cause of the increase in upward flow. Forsén (1985) found that at 0.6 wt% Ni and 0.47% wt% O, the anode microstructure consisted of a eutectic phase and NiO crystals. At lower oxygen concentrations the anode microstructure consisted of solid Cu and eutectic phases and NiO crystals. It is possible that the shift towards a eutectic phase alters the forming slime layer, which in turn would flow differently in the cell.

3.5. Effect of temperature on anode slime detachment

Based on the literature, higher temperatures are known to improve the adhesion of anode slimes on the anode with the peak adhesion temperature of 55-60 °C for high impurity anodes, and 65-70 °C for low impurity anodes (Zeng et al., 2015c). In this study, passivation was not observed at 60 °C and thus the detachment behaviour changed. No slime was seen to detach during the five days of electrolysis when the electrolyte Ni concentration was below 30 g/dm³ (EE-1.2, EE-2.2, EE-3.2, AE-1.2, AE-4.2). However, the slime layer was very fragile with all anode and electrolyte compositions. Even the slightest vibration in the experimental set-up could cause slime to detach in the form of clusters and individual particles. Increased temperature was expected to improve the settling rate, which it did for large clusters, which settled too fast to estimate the settling rate reliably. However, for individual particles, the increased temperature did not improve the settling rate, as can be seen from Fig. 16, which shows the vertical and horizontal velocity profiles of individual particles that detached due to vibration; the settling rates are very similar to the settling rates experienced at 25 °C.

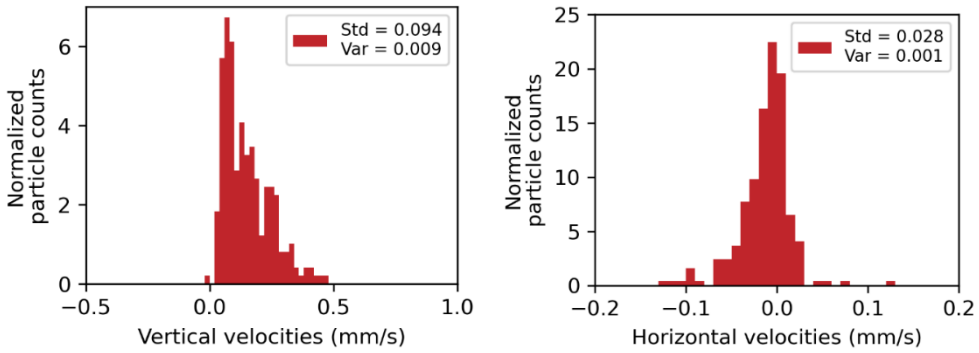

Fig. 16. Observed settling rates of anode slimes detaching due to vibrations around the experimental set-up

Increasing the nickel concentration of the electrolyte to 30 g/dm³ resulted in slime detachment even at elevated temperatures. The sizes of the detaching slime masses were approximately the same at 60 °C as at 25 °C, but the settling rate was significantly faster (>10 mm/s). Individual particles were observed to detach after two days of electrolysis at 350 A/m². Individual particles that detached from the anode surface at 60 °C sometimes became stuck in a gel-like substance that was visible on the anode surface (Fig. 4S). The composition and cause of the gel is unknown, but EE-4.2 where this was observed had a very high total sulphate concentration, due to having 30 g/dm³ Ni^{2+} added in the form of $NiSO_4$ and 200 g/dm³ H_2SO_4.

With longer experiments at elevated temperatures, *Avalanche* type detachment was anticipated (Fig. 2D) as it is the only form of detachment which is expected to be solely dependent on the mass and fragility of the anode slime layer; however, avalanches were never observed at elevated temperatures. In fact, in EE-4.2, where the nickel concentration was 30 g/dm³, the sulphuric acid concentration 200 g/dm³ and the temperature 60 °C, a few large clusters (>2 mm in diameter) were seen detaching from the anode surface towards the end of day 5 (Fig. 17 & 18). This further indicates that nickel concentration in the electrolyte leads to a more fragile slime layer, which detaches more easily. The detaching clusters did not affect the anode potential, nor was the entire slime layer removed. The exact causes of slime detachment in ideal electrorefining conditions at elevated temperatures are unknown. It could be that the sulphuric acid degrades the slime layer, and as a result the outer layer is more fragile and detaches. It is known that the inner layer has a slightly higher temperature, and it is possible that

the sulphates which precipitate on the outer layer could cause the structure to collapse. In an industrial environment a more fragile layer is likely to detach more easily. From the results it is evident that increasing the amount of Ni^{2+} and H_2SO_4 can cause a more fragile anode slime layer, thus increasing the risk of cathode contamination due to suspended and slowly settling anode slime particles.

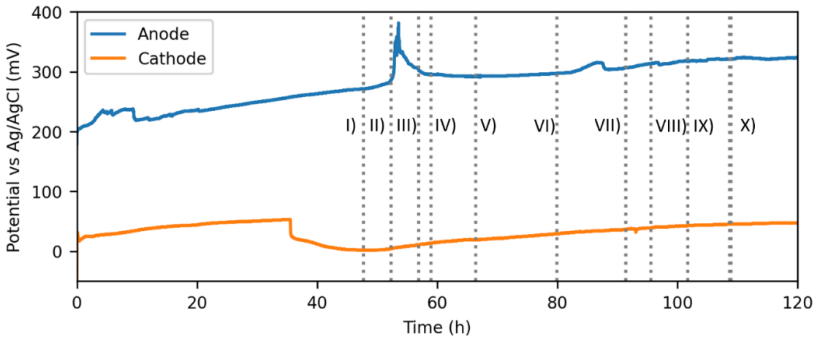

Fig. 17. Anode and cathode potentials as a function of time in electrorefining with high nickel concentration (EE-4.2). Vertical lines I to X represent observed slime detachment times. I-VII) A few individual microscopic and 0.1-0.5 mm sized particles detaching from the anode and settling straight down. VIII) 1-2 mm slime clusters detach. IX) Individual particles detach. X) 2-4 mm slime cluster collapses from the anode surface

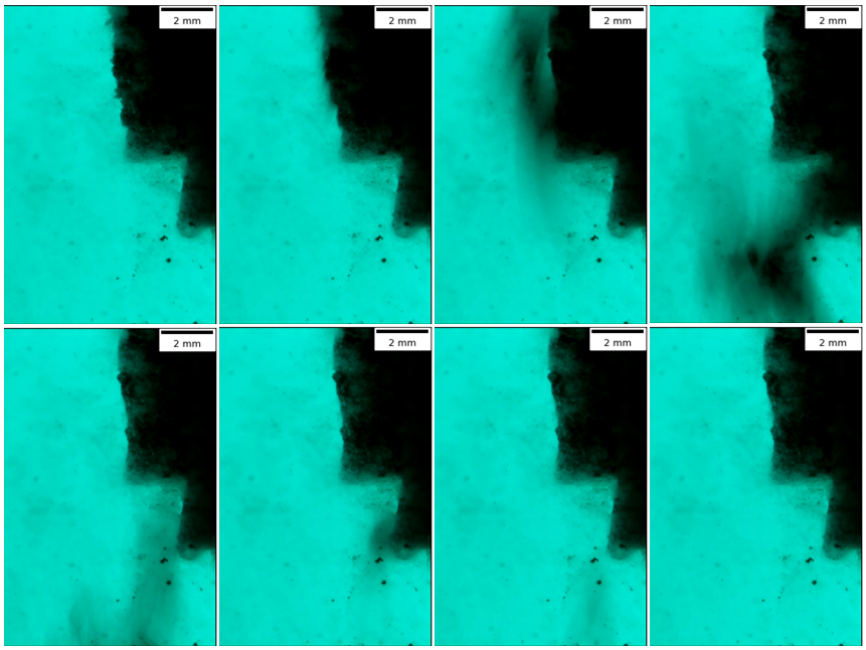

Fig. 18. Anode slime detachment by *Avalanche* (point X) from Fig. 17). Each frame represents 0.1 seconds of electrolysis

4. Conclusions

Anode slimes detach from anode surfaces by four mechanisms: *cloud formation*, *individual particles*, *cluster detachment* or *avalanche*. In our study, *cloud formation* was mainly associated with high impurity anodes. *Individual particles* detached in all conditions, but *cluster detachment* was more common with high impurity anodes than with low impurity anodes. It should be noted that high impurity anodes generate more slime and clusters may require a certain amount of slime to form. Given a longer time period, it could be that low impurity anodes would also start generating more clusters. For the most part, the settling trajectories are relatively straight, and particles go either up or down; however, at times the particles can be trapped in vortexes and or move in random directions without any obvious cause. Prediction of individual particle trajectories and velocities is impossible, but as the sample size increases the particle velocities follow a normal distribution. Horizontal velocities are typically in the range of -0.2

to 0.2 mm/s (negative value indicating that movement is towards the cathode) and vertical velocities are typically in the range of -0.5 to 1.0 mm/s (negative value indicating upward flow). Despite the impossibility of predicting exact slime behaviour, it can be concluded that:

- In the absence of external flow, the settling slime particles do not become entrapped in the natural convection. Anode slime settling velocities are typically in the range of -0.5-1.0 mm/s, despite changes in electrolyte composition or operating temperature. At 60 °C, large slime clusters exceed these velocities.
- Higher sulphuric acid concentration degrades the structural integrity of the anode slime layer, leading to anode slime detachment favouring individual particles and smaller anode slime clusters. From the plant operation point of view this might be favourable as some authors have suggested that particle size is the determining factor in cathode nodulation (Dutrizac and Chen, 1999).
- The results support the fact that increasing the nickel concentration of the electrolyte promotes formation of a more porous slime layer on the anode surface. At lower (100 g/dm^3) sulphuric acid concentrations this leads to more upward flowing slimes, but at higher (200 g/dm^3) sulphuric acid concentrations the more porous structure might aid in degrading the slime layer.
- Anode nickel significantly increases the upward flow of anode slimes, increasing the probability of cathode contamination.
- Anode oxygen concentration does not seem to affect the flow behaviour of anode slimes at lower oxygen concentrations (<0.44 wt%).
- Increasing the temperature to 60 °C eliminates passivation, reduces the presence of anode slime in the electrolyte and leads to individual particles and clusters detaching from the anode surface. The slime layer is very fragile and, in real operations, even slight vibrations caused by moving operators and equipment may lead to slime detaching from the surface.

While the majority of settling anode slimes are <0.1 mm in diameter, new findings suggest that detaching anode slimes can form clusters with a diameter of up to 7 mm, and that particle clusters of 1 mm in diameter are not uncommon. In addition, the increased slime particle and cluster sizes do not necessarily lead to faster settling. These large clusters are unlikely to stick to the cathodes as intact clusters; instead, they break apart upon contact and potentially cause significant contamination and nodulation. More research should also be carried out on the effect of anode mineralogy on slime detachment, slime adhesion and anode slime flow behaviour in an electrorefining cell. Since the anode casting process has an impact on the anode mineralogy, there may be opportunities for improving the settling behaviour of slimes by adjusting the casting process appropriately, rather than achieving better settling by adding further additives to the electrolyte.

Acknowledgments

This work made use of the RawMaTTERS Finland Infrastructure (RAMI) funded by the Academy of Finland and based at Aalto University. The calculations presented above were performed using computer resources within the Aalto University School of Science "Science-IT" project. This work was supported by the Towards Carbon Neutral Metals project (TOCANEM), funded by Business Finland (grant no. 40693/31/2020). Boliden Harjavalta Oy funded the research and provided industrial anodes for this work. Some of the initial results of this work were previously presented in the proceedings of the Copper-Cobre 2022 conference on November 13-17th 2022 in Santiago de Chile.

References

ABE, S., BURROWS, B. W., ETTEL, V. A., 1980. *Anode Passivation in Copper Refining*. Can. Metall. Q. 19(3), 289–296. Available at: https://doi.org/10.1179/cmq.1980.19.3.289.

ALLAN, D. B., CASWELL, T., KEIM, N. C., VAN DER WEL, C. M., VERWEIJ, R. W., 2021. *soft-matter/trackpy: Trackpy v0.5.0.* Zenodo. Available at: https://doi.org/10.5281/zenodo.4682814.

ANDERSEN, T. N., PITT, C. H., LIVINGSTON, L. S., 1983. *Nodulation of electrodeposited copper due to suspended particulate*. J. Appl. Electrochem. 13(4), 429–438. Available at: https://doi.org/10.1007/BF00617517.

CHEN, T. T., DUTRIZAC, J. E., 1990. *A Mineralogical overview of the behavior of nickel during copper electrorefining*. Metall. Trans. B. 21(2), 229–238. Available at: https://doi.org/10.1007/BF02664190.

DUAN, H., HOU, K., LI, J., ZHU, X., 2011. *Examining the technology acceptance for dismantling of waste printed circuit boards in light of recycling and environmental concerns*. J. Environ. Manage. 92(3), 392–399. Available at: https://doi.org/10.1016/j.jenvman.2010.10.057.

DUTRIZAC, J. E., CHEN, T. T. A., 1999. *A mineralogical study of nodulated copper cathodes.* in Proceedings of Copper 99-Cobre 99 International Conference. Vol.III Electrorefining and Electrowinning of Copper. 383–404.

FORSÉN, O., 1985. *The behaviour of nickel and antimony in oxygen-bearing copper anodes in electrolytic refining*. Doctoral Dissertation, Helsinki University of Technology.

GU, Z. H., CHEN, J., FAHIDY, T. Z., 1995. *A study of anodic slime behaviour in the electrorefining of copper*. Hydrometallurgy. 37(2), 149–167. Available at: https://doi.org/10.1016/0304-386X(94)00044-4.

HANUS, D., 1987. *Influence of Composition and Passivation of Anodes on Sludge Properties* (Wpływ składu i pasywacji anod na właściwości szlamu). Pr. Inst. Met. Niezelaz. 16, 35–39

International Copper Study Group, 2022. *The World Copper Factbook 2022*.

JARJOURA, G., KIPOUROS, G. J., 2006a. *Effect of nickel on copper anode passivation in a copper sulfate solution by electrochemical impedance spectroscopy*. J. Appl. Electrochem. 36(6), 691–701. Available at: https://doi.org/10.1007/s10800-006-9130-2.

JARJOURA, G., KIPOUROS, G. J., 2006b. *Electrochemical studies on the effect of nickel on copper anode passivation in a copper sulphate solution*. Can. Metall. Q. 45(3), 283–294. Available at: https://doi.org/10.1179/cmq.2006.45.3.283.

KALLIOMÄKI, T., AJI, A. T., RINTALA, L., AROMAA, J., LUNDSTRÖM, M., 2017. *Models for viscosity and density of copper electrorefining electrolytes*. Physicochem. Probl. Miner. Process. 53(2), 1023–1037. Available at: https://doi.org/10.5277/ppmp170227.

KALLIOMÄKI, T., AJI, A. T., AROMAA, J., LUNDSTRÖM, M., 2019. *Settling properties of copper electrorefining anode slimes*. in Proceedings of the 58th Annual Conference of Metallurgists (COM) Hosting the 10th International Copper Conference 2019.

LING, X., GU, Z. H., FAHIDY, T. Z., 1994a. *Anode slime behaviour in a laboratory-scale copper electrorefining process*. Can. J. Chem. Eng. 72, 683–694.Available at: https://doi.org/10.1002/cjce.5450720418.

LING, X., GU, Z. H., FAHIDY, T. Z., 1994b. *Effect of operating conditions on anode passivation in the electrorefining of copper*. J. Appl. Electrochem. 24(11), 1109–1115. Available at: https://doi.org/10.1007/BF00241308.

MICHAUX, S.P., 2021. *The Mining of Minerals and the Limits to Growth*. 16/2021. Geological Survey of Finland. Available at: https://tupa.gtk.fi/raportti/arkisto/16_2021.pdf (Accessed: 27 January 2023).

MIIKKI, K. AND KARAKOC, A., 2020. *kmiikki/rpi-camera: RPI-camera-software-suite*. Zenodo. Available at: https://doi.org/10.5281/zenodo.4275964.

MOATS, M., FILZWIESER, A., DAVENPORT, W. G., ABEL, R., WANG, S., 2022. *Global Survey of Copper Electrorefining: 2022 World Tankhouse Operating Data.* in Proceedings of Copper - Cobre 2022 International Conference vol. 5: Electrometallurgy, 64-74.

MOATS, M. S., 1998. *Electrochemical Characterization of Anode Passivation Mechanism in Copper Electrorefining*. Doctoral Dissertation, The University of Arizona.

OGAWA, K., 2016. *Copper Electrowinning and Nickel Recovery from Black Copper Containing High Levels of Impurities from the Smelting Process of Complex Recycling Materials*. in Proceedings of the International Copper Conference 2016.

SAHLMAN, M., AROMAA, J., LUNDSTRÖM, M., 2021. *Copper Cathode Contamination by Nickel in Copper Electrorefining*. Metals 11, 1758. Available at: https://doi.org/10.3390/met11111758.

SAHLMAN, M., AROMAA, J., LUNDSTRÖM, M., 2022. *The effect of electrolytic nickel on the anode slime detachment from the anode surface*. in Proceedings of Copper - Cobre 2022 International Conference vol. 5: Electrometallurgy, 85-97.

TETSUKA, D., OKAMOTO, H., 2019. *Effect of Antimony, Nickel and Sulfuric Acid in Copper Electrorefining*. in Proceedings of the 58th Annual Conference of Metallurgists (COM) Hosting the 10th International Copper Conference 2019.

ZENG, W., FREE, M. L., WERNER, J., WANG, S., 2015a. *Simulation and Validation Studies of Impurity Particle Behavior in Copper Electrorefining*. J. Electrochem. Soc. 162, E338. Available at: https://doi.org/10.1149/2.0561514jes.

ZENG, W., FREE, M. L., WANG, S., 2015c. *Studies of Anode Slime Sintering/Coalescence and Its Effects on Anode Slime Adhesion and Cathode Purity in Copper Electrorefining*. J. Electrochem. Soc. 163, E14. Available at: https://doi.org/10.1149/2.0681602jes.

ZENG, W., WANG, S., FREE, M. L., 2016a. *Experimental and Simulation Studies of Electrolyte Flow and Slime Particle Transport in a Pilot Scale Copper Electrorefining Cell*. J. Electrochem. Soc. 163, E111. Available at: https://doi.org/10.1149/2.0181605jes.

ZENG, W., WANG, S., FREE, M. L., 2016b. *Experimental Studies of the Effects of Anode Composition and Process Parameters on Anode Slime Adhesion and Cathode Copper Purity by Performing Copper Electrorefining in a Pilot-Scale Cell*. Metall. Mater. Trans. B 47(5), 3178–3191. Available at: https://doi.org/10.1007/s11663-016-0736-4.

ZENG, W., WANG, S., FREE, M. L., 2017. *Two-Phase Flow Modeling of Copper Electrorefining Involving Impurity Particles*. J. Electrochem. Soc. 164(9), E233. Available at: https://doi.org/10.1149/2.0401709jes.

ZENG, W., WERNER, J., FREE, M. L., 2015b. *Experimental studies on impurity particle behavior in electrolyte and the associated distribution on the cathode in the process of copper electrorefining*. Hydrometallurgy. 156, 232–238. Available at: https://doi.org/10.1016/j.hydromet.2015.06.005.

Supplementary material

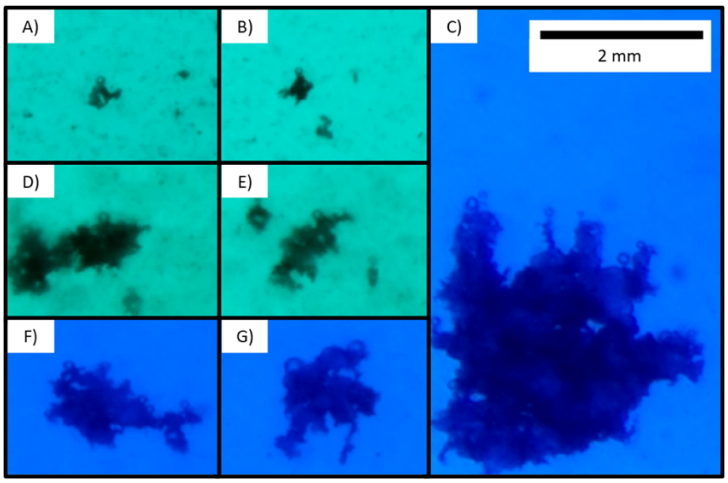

Fig. 1S. Examples of bubbles attached to anode slime clusters of various sizes. A and B are from experiments EE-3. D and E are from experiment CEE-3. C, F and G are from experiment AE-5

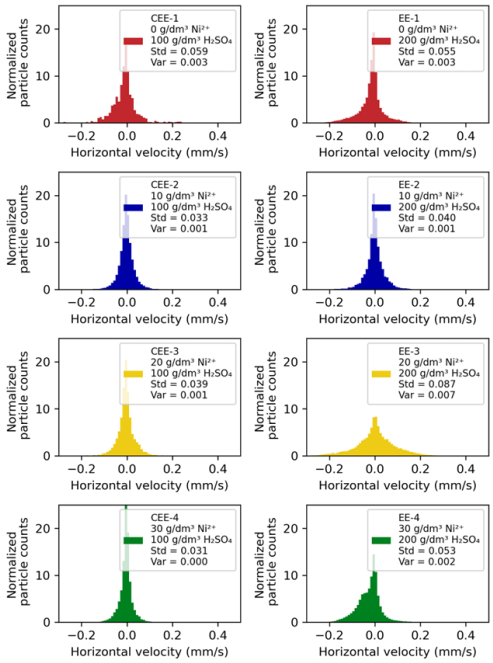

Fig. 2S. Horizontal velocity profiles of anode slimes with and electrolyte composition of 40 g/dm³ Cu^{2+} and a temperature of 25°C. Negative velocity indicates movement is towards the cathode and a positive velocity indicates that the movement is towards the anode

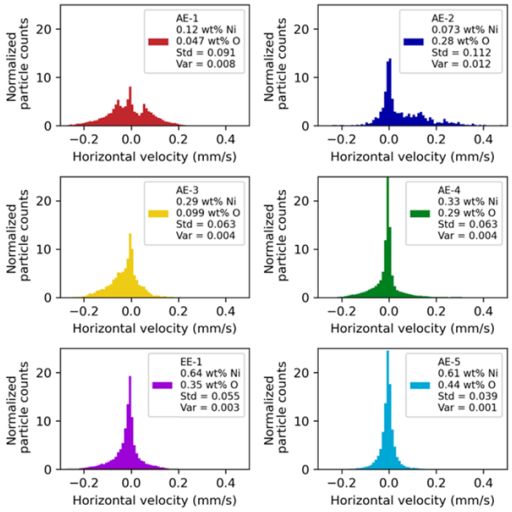

Fig. 3S. Horizontal velocity profiles of anode slimes with and electrolyte composition of 40 g/dm³ Cu^{2+}, 200 g/dm³ H_2SO_4 and a temperature of 25°C. Negative velocity indicates movement is towards the cathode and a positive velocity indicates that the movement is towards the anode

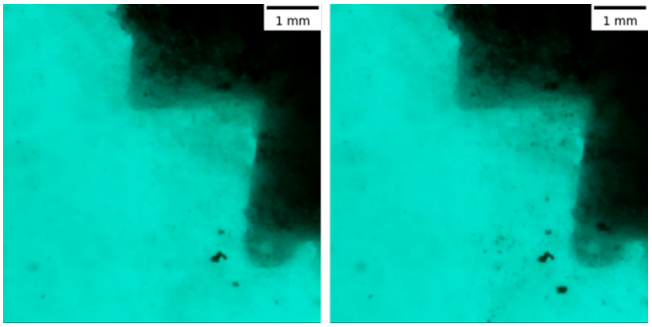

Fig. 4S. Frame 3661392 (left) and frame 3661992 (right) representing 6 minutes of electrolysis done in EE-4.2. Miniscule particles have detached from the anode slime surface, but instead of settling, they've adhered to something gel-like on the anode surface

Table 1S. Statistics on total velocities of observed trajectories at 25°C

Experiment	Max velocity (mm/s)	Min velocity (mm/s)	Average velocity (mm/s)	Median velocity (mm/s)	Standard deviation (mm/s)	Variance
CEE-1	1.822	0.003	0.257	0.154	0.255	0.0648
CEE-2	1.600	0.002	0.148	0.107	0.133	0.0176
CEE-3	1.578	0.004	0.201	0.133	0.18	0.0324
CEE-4	1.786	0.002	0.167	0.107	0.161	0.0259
EE-1	1.473	0.001	0.159	0.123	0.123	0.0152
EE-2	1.687	0.001	0.180	0.139	0.146	0.0214
EE-3	1.628	0.001	0.152	0.124	0.108	0.0118
EE-4	1.597	0.001	0.139	0.100	0.123	0.015
EE-5	1.853	0.001	0.209	0.154	0.187	0.0351
AE-1	1.554	0.001	0.123	0.099	0.0917	0.00841
AE-2	1.655	0.003	0.205	0.152	0.199	0.0398
AE-3	1.807	0.001	0.174	0.113	0.188	0.0353
AE-4	1.737	0.001	0.151	0.114	0.124	0.0153
AE-5	1.680	0.002	0.142	0.095	0.135	0.0181

Table 2S. Statistics on horizontal velocities of observed trajectories at 25°C. Negative sign indicates that the movement is towards the cathode and positive sign indicates that the movement is towards the anode

Experiment	Max velocity (mm/s)	Min velocity (mm/s)	Average velocity (mm/s)	Median velocity (mm/s)	Standard deviation (mm/s)	Variance
CEE-1	0.252	-0.705	-0.011	-0.008	0.0591	0.00349
CEE-2	0.386	-0.290	-0.003	-0.003	0.0333	0.00111
CEE-3	0.275	-0.352	-0.005	-0.005	0.0394	0.00155
CEE-4	0.326	-0.417	-0.005	-0.003	0.0311	0.000964
EE-1	0.464	-0.408	-0.017	-0.010	0.0551	0.00303
EE-2	0.289	-0.270	-0.001	-0.001	0.0405	0.00164
EE-3	0.736	-0.476	0.003	0.002	0.0876	0.00767
EE-4	0.609	-0.780	-0.026	-0.017	0.0539	0.00291
EE-5	0.686	-1.007	-0.002	-0.003	0.0799	0.00638
AE-1	0.622	-0.364	-0.010	-0.010	0.0911	0.0083
AE-2	0.811	-0.234	0.059	0.013	0.113	0.0127
AE-3	0.355	-0.350	-0.028	-0.017	0.0638	0.00407
AE-4	0.738	-0.300	-0.009	-0.006	0.0638	0.00407
AE-5	0.465	-0.487	-0.005	-0.004	0.0393	0.00155

Table 3S. Statistics on vertical velocities of observed trajectories at 25°C. Negative sign indicates that the movement is towards the electrolyte surface and positive sign indicates that the movement is towards the bottom of the electrorefining cell

Experiment	Max velocity (mm/s)	Min velocity (mm/s)	Average velocity (mm/s)	Median velocity (mm/s)	Standard deviation (mm/s)	Variance
CEE-1	1.816	-0.751	0.233	0.148	0.271	0.0732
CEE-2	1.598	-0.587	0.142	0.103	0.135	0.0182
CEE-3	1.577	-0.524	0.171	0.125	0.205	0.0419
CEE-4	1.546	-1.785	0.119	0.093	0.197	0.0387
EE-1	1.473	-1.102	0.097	0.089	0.167	0.0278
EE-2	1.687	-0.794	0.151	0.123	0.171	0.0293
EE-3	1.617	-0.897	0.085	0.077	0.142	0.02
EE-4	1.597	-1.560	0.089	0.070	0.151	0.023
EE-5	1.852	-1.636	0.165	0.120	0.212	0.045
AE-1	1.419	-1.552	0.065	0.048	0.105	0.011
AE-2	1.654	-0.537	0.160	0.100	0.2	0.04
AE-3	1.807	-0.423	0.133	0.078	0.207	0.0431
AE-4	1.737	-1.694	0.106	0.089	0.15	0.0225
AE-5	1.676	-1.220	-0.014	-0.061	0.191	0.0365